J. Biomedical Science and Engineering, 2014, 7, 157-172
Published Online March 2014 in SciRes. http://www.scirp.org/journal/jbise
http://dx.doi.org/10.4236/jbise.2014.74020

Scientific Research

Optimization of Image Quality in Retrospective Respiratory-Gated Micro-CT for Quantitative Measurements of Lung Function in Free-Breathing Rats

Nancy L. Ford[1,2], Andrew Jeklin[1], Karen Yip[2], Darren Yohan[2], David W. Holdsworth[3], Maria Drangova[3]

[1]Department of Oral Biological and Medical Sciences, The University of British Columbia, Vancouver, Canada
[2]Department of Physics, Ryerson University, Toronto, Canada
[3]Schulich School of Medicine & Dentistry, The University of Western Ontario, London, Canada
Email: nlford@dentistry.ubc.ca

Received 30 January 2014; revised 2 March 2014; accepted 9 March 2014

Abstract

Objective: To optimize scan time and X-ray dose with no loss of image quality for retrospectively-gated micro-CT scans of free-breathing rats. Methods: Five free-breathing rats were scanned using a dynamic micro-CT scanner over 10 continuous gantry rotations (50 seconds and entrance dose of 0.28 Gy). The in-phase projection views were selected and reconstructed, representing peak inspiration and end expiration from all 10 rotations and progressively fewer rotations. A least error method was also used to ensure that all angular positions were filled. Image quality and reproducibility for physiological measurements were compared for the two techniques. Results: The least error approach underestimated the lung volume, air content in the lung at peak inspiration, and tidal volume. Other measurements showed no differences between the projection-sorting techniques. Conclusions: Seven gantry rotations (35 seconds and 0.2 Gy dose) proved to be the optimal protocol for both the in-phase images and the least error images.

Keywords

Respiratory-Gating; Micro-CT; Lung Imaging; Free-Breathing Rats; Tidal Volume

1. Introduction

Micro-computed tomography techniques have been developed and reported for non-invasive monitoring of var-

How to cite this paper: Ford, N.L., Jeklin, A., Yip, K., Yohan, D., Holdsworth, D.W. and Drangova, M. (2014) Optimization of Image Quality in Retrospective Respiratory-Gated Micro-CT for Quantitative Measurements of Lung Function in Free-Breathing Rats. *J. Biomedical Science and Engineering*, **7**, 157-172. http://dx.doi.org/10.4236/jbise.2014.74020

ious respiratory diseases modeled in rodents [1]-[7]. To obtain structural and functional information from the images, respiratory-gated imaging at multiple time points in the respiratory cycle is required. Both prospective [8]-[11] and retrospective [12]-[14] techniques have been previously reported. Prospective gating techniques ensure that all projection views are acquired in the desired respiratory phase; however, multiple image acquisitions of different respiratory phases are required to provide sufficient data to measure lung function. Retrospective gating acquires projection views throughout the respiratory cycle, with the projections sorted based on the phase of the respiratory cycle the animal was in when the projection was acquired. Although any portion of the respiratory cycle can be reconstructed, some of the data will be discarded because it is not in the desired phase, which may lead to missing view artefacts in the image or increased X-ray dose to the animal due to acquiring redundant projections for a given phase in the cycle.

Using the respiratory-gated images, anatomical measurements can be made with reduced motion artefacts and uncertainties due to organ motion for the desired respiratory phase. Semi-automated and fully automated algorithms to extract and/or classify features, such as airways or vessels, have been described [15]-[19]. In all of these studies, the ability to accurately measure lung morphology is dependent on good motion reduction (gating), low image noise and for the greyscale-based algorithms, accurate and reproducible grey scale values.

For prospective gating, the image quality is the same for all images—one simply has to wait for the animal to reach the desired respiratory phase at each angular position before acquiring the projection. In the case of retrospectively gated images, the number of unique projection views in each respiratory phase will be dependent upon the respiratory rate, how stable the rate remains throughout the scan, and on the respiratory phase at the beginning of the scan. Therefore retrospectively gated images are more susceptible to variability in the image quality achieved, leading to more difficulties in measuring the morphology with the semi-automated and automated algorithms. One major downfall of the threshold-based segmentation algorithms occurs for images with poor signal-to-noise and/or missing view artefacts; in these cases, the segmentation algorithms will leak out of the desired region into the surrounding tissue causing an artificially increased volume to be extracted.

For retrospective gating, improvements in the projection selection algorithms may improve the signal-to-noise ratio and reduce or eliminate artefacts due to missing projection views and respiratory motion. Ford *et al.* describe a method using a temporal window positioned at a specific portion of the externally monitored respiratory trace to select the projections that were acquired during the desired respiratory phase [12]. Since the respiratory trace was based on the motion of the diaphragm monitored externally, the motion of the diaphragm and the recorded trace may not be perfectly synchronized. Furthermore, for free-breathing animals, the portion of the trace that is included in the window may be slightly different from breath-to-breath. An alternate means of retrospectively gating uses information from the projection views to determine the respiratory phase during which the projection was acquired. Hu *et al.* used the diaphragm position to select projections [13], whereas Ertel *et al.* measured diaphragm motion with a Kymogram function to select projections from the desired respiratory phase [14]. Ertel demonstrated a reduction in blurring with good temporal efficiency using the Kymogram technique. Armitage *et al.* implemented a least error method to ensure that all angular positions were filled in the reconstructed image [20]. In this approach, redundant projections are required at each angle, and some of the angular positions may not exactly be in the same respiratory phase, but image quality metrics showed an improvement for phantom images.

In this paper, we aim to optimize our previously reported [12] scanning protocols for retrospectively respiratory-gated micro-CT imaging for rats to reduce the imaging time and X-ray dose to the animal. We also investigate the effects of including projection views that are not quite in phase to completely fill projection space and eliminate missing view artefacts in the resulting images. Quantitative measurements of image quality and physiologically relevant metrics will be performed in the images using only in-phase projections and compared with those images that add nearly in-phase projections to completely fill projection space.

2. Materials and Methods

2.1. Animal Model

Five healthy male Sprague-Dawley rats (mean mass = 381 ± 16 g) were housed in a pathogen-free vivarium, with access to water and standard rodent chow ad libitum. For the experimental protocol, each rat was anaesthetized with an intra-peritoneal injection of a mixture of 80 mg/kg ketamine and 5 mg/kg xylazine. Throughout the experiments, the rats were free-breathing, and their respiration and body temperatures were monitored conti-

nuously. All animal procedures were approved by the Animal Use Subcommittee at the University of Western Ontario.

2.2. Micro-Computed Tomography Scanning

During the scanning protocol, the animals were free-breathing but under anaesthesia. The micro-CT scanner was a high-speed, cone beam CT scanner (Locus Ultra, General Electric HealthCare, London, Canada), which has been characterised previously [21]-[23]. The scanning protocol acquired 4160 projection views over 10 continuous gantry rotations at 80 kVp and 50 mA with a 50 s X-ray exposure time (5 s per gantry rotation), in accordance with the optimized exposure settings described by Du *et al.* [23]. The acquisition time for each projection was 12 ms. The entrance dose for this protocol has been measured previously and is approximately 0.28 Gy in air at scanner isocentre [12]. For calibration purposes, a small tube of water is included in each image to convert the recorded signal intensities into Hounsfield units.

During the scan, the respiration signal and the rectal temperature were continuously monitored and recorded using a rodent physiological monitoring system (Biovet, m 2 m Imaging Corp., Cleveland, USA). The animal was positioned prone on the CT imaging bed, with a pneumonic pillow positioned under the diaphragm. The animal was free-breathing and the motion of the diaphragm caused a measurable change in pressure in the pillow, which was used as a surrogate for the respiratory trace. In addition, a signal indicating when the x-ray beam was switched on was routed from the micro-CT scanner and recorded using the Biovet system to establish a common timeframe between the respiratory waveform and the acquisition of the projection views.

Each animal received 3 micro-computed tomography scans in a single imaging session. Upon reviewing the respiratory traces, we found that some gasps occurred during the imaging sessions, which allowed the projection-sorting algorithm to select inappropriate projections. To eliminate this source of error, we identified 2 scans for each rat that demonstrated reproducible respiratory patterns for further analysis.

2.3. Retrospective Respiratory Sorting

A retrospective respiratory-sorting algorithm was used to identify the projections that were acquired during each desired phase of the respiratory cycle. Retrospectively sorting the projection data allows images to be reconstructed at any phase of the respiratory cycle from a single acquisition; however, since some of the projection views are rejected because they are not in the specified phase, the images may suffer from reduced image quality if projection space is not completely filled. To assess the effects of missing view artefacts in the images, we reconstructed each dataset using two respiratory sorting techniques, in-phase and least error, outlined below.

In-phase: In this approach, only the projection views that were acquired during the desired phase were included in the reconstruction, which may result in missing views in the reconstruction. For each micro-CT scan, the projections were sorted into end expiration and peak inspiration phases based on a threshold approach. The end expiration segments of the respiratory trace were defined as all time points during the respiratory trace where the recorded signal was less than 20% of the full range of recorded values. Peak inspiration was defined as those time points in the respiratory trace with signal values greater than 80% of the full range. For each phase, the projection views that were acquired during the defined periods were included in the respiratory-sorted set, including projections from all 10-gantry rotations.

Least Error: In the least error respiratory-sorting approach, the time between the acquisition of the projection views and the desired respiratory phase is calculated. For each angular position, the projection view that was acquired with a time closest to the desired phase was used in the reconstruction. This sorting technique ensures all projection angles are filled and has been described previously by Armitage *et al.* [20].

In addition to the respiratory-gated images, ungated images were also reconstructed for each micro-CT scan. In the ungated case, all projection views from the first gantry rotation were used for reconstruction.

2.4. Image Reconstruction

Images representing the ungated image and the respiratory-gated images for peak inspiration and end expiration using each sorting approach were reconstructed. A Feldkamp-type [24] cone beam reconstruction algorithm was implemented to produce 3D volumetric images with isotropic voxel spacing of 0.15 mm. The algorithm requires that the angular position at which each projection was acquired is accurately known, but does not require even sampling intervals. For each image, only the unique projection views were reconstructed for a maximum of 416

valid projection views; duplicate views at the same angular position from subsequent gantry rotations were discarded regardless of the respiratory phase during which they were acquired. For the in-phase reconstructions, it was possible for the reconstructed image to include fewer than 416 views, depending on the respiratory patterns exhibited during the scan. The least error sorting approach guaranteed 416 views for reconstruction, although some fractions of these projection views were not acquired during the desired respiratory phase.

Using a similar approach to our previous work describing an optimized retrospective gating technique for use with mice [12], we optimized the protocol for imaging the lungs of rats to improve measurements of physiologically relevant parameters with minimal loss of image quality. In the previous mouse study, we only included in-phase projections in the reconstructed images. Optimization of the technique is needed for different species due to the differences in respiratory rates. To optimize the technique for rats, we simulated scanning with fewer gantry rotations, implying fewer projections acquired but with a shorter scan-time and lower dose. We reconstructed images using all 10 rotations, using the first 9 rotations, and so on down to 3 rotations, at which point the image quality suffered from too few projections acquired in the desired respiratory phase. We reconstructed images using continuous gantry rotations ranging from 3 to 10 to optimize between the image quality, scan time and x-ray dose delivered to the animal for both sets of images (in-phase and least error) gated to peak inspiration and to end expiration.

Images were rescaled into Hounsfield units, where the pixel values representing air in the trachea were set to −1000 HU and those representing the water in the calibration tube were set to 0 HU. The ungated images were reoriented to align the major airways with the axes of the image, and the same co-ordinate transform was applied to reorient all of the gated images from the same acquisition.

2.5. Image Analysis

Image analysis metrics can be separated into two categories: image quality and physiological measurements. For each image, the same measurements were performed and values were compared within each sorting approach for 3 - 10 continuous gantry rotations. A second comparison was done between the 10-rotation in-phase image (considered to be the gold standard) and each of the least error images for 3 - 10 gantry rotations. The 10-rotation image was considered to be the gold standard since it had the most projection views filled with the in-phase conditions. All image-based analysis was performed using MicroView Analysis+ (v2.2, General Electric Healthcare, London, Canada).

Image Quality: Similar to our previously published work [12], we measured the photon noise in the image by calculating the standard deviation in a region of interest inside the heart (mean ROI volume = 440 ± 4 mm^3). Missing view artefacts were measured in a region of interest (mean ROI volume = 1857 ± 13 mm^3) in air above the animal's spine and corrected to remove the photon noise contribution as described in Equation (1) [12]:

$$\sigma_{MVA,n} = \sqrt{\sigma_{ROI}^2 - \sigma_{\text{photon,ungated}}^2 \frac{v_{\text{ungated}}}{v_n}} \tag{1}$$

where σ_{ROI} is the measured standard deviation in the region of interest, $\sigma_{\text{photon, ungated}}$ is the photon noise measured in the ungated image, v_{ungated} is the number of views in the ungated image (416) and v_n is the number of projection views used to form the gated image.

Physiological Measurements: Using the 10-rotation expiration images, the threshold value was found by selecting a region of interest containing approximately 50% soft tissue and 50% lung tissue. An automated algorithm [25] was used to identify the grey-scale value that separated the lung tissue from the background soft tissue. The threshold value (−237 HU) was obtained as the average for all 5 rats and was applied to all images. Using a seeded region-growing algorithm, we extracted the whole lung by selecting pixels with grey scale values below the threshold (−237 HU). For each region of interest, the volume and mean CT number were calculated.

Functional parameters were calculated from the image-based measurements. The functional residual capacity (FRC) is given in Equation (2), and the tidal volume (V_t) in Equation (3), where the volumes are measured in millilitres and the densities in Hounsfield units. Each of these equations accounts for the fractional air content in the lungs [18] [26]-[28].

$$FRC = \text{Volume}_{\text{expiration}} \times \left(\frac{\text{mean lung density}_{\text{expiration}}}{\text{air density}} \right) \tag{2}$$

$$V_t = \text{Volume}_{\text{peak inspiration}} \times \left(\frac{\text{mean lung density}_{\text{peak inspiration}}}{\text{air density}} \right) - FRC \quad (3)$$

To assess the accuracy of the gating in the images created from the least error respiratory sorting approach, we analysed the sharpness of the diaphragm at 4 locations in a coronal plane corresponding to the midline of the lungs. Corresponding images from the in-phase sorting approach were also analysed and the line profiles compared between the images. For this analysis, only one scan for each rat was used due to the extreme amounts of data generated. The planes were selected to be as close as possible to the same location for all of the rats, and were identical between the images from the same acquisition. For each image, four lines 9 mm in length were drawn straddling the diaphragm. The lines were aligned with the image axis and were located near the medial edge and near the lateral edge of the right and left lobes as shown in **Figure 1**, crossing the diaphragm approximately perpendicular to the bottom edge of the lung. The profiles were aligned at the position with the highest gradient to account for slight differences in positioning the profile lines between images. The profile lines were plotted and the slope and shape of the line were taken as qualitative indicators of diaphragm sharpness. To exclude the shoulders of the curve, the slope of the line of best fit through each profile was calculated for the portion of the curve extending 3 mm on either side of the point with the highest gradient.

2.6. Statistical Analysis

Statistical analysis was performed using Prism (v4.0c, Graph Pad Software, Inc., San Diego, USA). To compare the images made from 3 - 10 continuous gantry rotations with the same respiratory sorting approach, a repeated measure ANOVA with Dunnett's post hoc test was performed. For this comparison, measured values from each image were compared to those from the image produced using all 10-gantry rotations. To compare between the two respiratory sorting techniques, images were compared to the 10-gantry rotation in-phase image, using the same statistical methodology. We report the mean values with the standard error in the mean (mean ± SEM), considering p-values < 0.05 as being significant.

3. Results

3.1. Respiratory Sorting

In retrospectively gated scans, the number of projection views that are used for a reconstruction depends on the respiratory rate of the animal. Although the rats in this study were allowed to breathe freely, their respiratory traces showed that the rates were consistent throughout the scans. The mean respiratory rate recorded was 83 ± 20 breaths per minute. Based on these measured respiratory traces, the temporal windows identified in peak inspiration and end expiration varied in length for different rats, and for subsequent scans of the same rat. For the

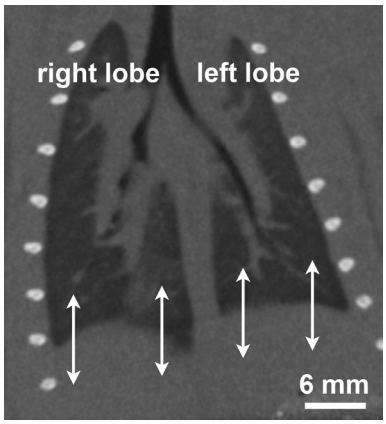

Figure 1. Sample line profiles drawn on a coronal slice. The lines were drawn 9 mm in length approximately perpendicular to the diaphragm with 2 lines on each lobe.

acquisition window corresponding to peak inspiration, the mean window length was calculated for each rat, and ranged between 87 ms to 117 ms, while the end expiration window length ranged from 271 ms to 645 ms.

3.2. Qualitative Image Analysis

Figure 2 shows the multiplanar reformatted images from a single animal where the projections were selected from all ten-gantry rotations. The coronal images in panels a) and b) are the end expiration and peak inspiration images reconstructed with least error approach, and panels c) and d) depict end expiration and peak inspiration images respectively using only the in-phase projections.

In **Figure 3**, the multiplanar reformatted images are shown at each respiratory phase (peak inspiration and end expiration) in the same rat using only the projections acquired in the first three gantry rotations to reconstruct the image. The coronal images in panels a) and c) are the end expiration images and b) and d) depict the peak inspiration images. Panels a) and b) used the least error approach to completely fill projection space, whereas panels c) and d) were reconstructed using only the in-phase projections.

In-phase images reconstructed from fewer gantry rotations have fewer projections in the desired phase and therefore exhibit streak artefacts due to the missing projection views, as seen when comparing **Figures 2** and **3**. Image noise is noticeably increased at both respiratory phases in **Figure 3**. End expiration images exhibit better image quality than the corresponding peak inspiration images due to an increased number of projections included. Since all of the projection angles are filled in the images reconstructed by the least error method, the streak artefacts are eliminated and the noise in the images is comparable for all 4 panels (**Figures 2(c)** and **(d)**, **Figures 3(c)** and **(d)**). **Figure 4** shows the axial images corresponding to a slice at the level of the 4th rib in the coronal images. In the axial plane, the missing view artefact is more noticeable for the in-phase reconstructions.

3.3. Image Quality Measurements

Measured values for the mean and standard error in the mean for the image noise and missing view artefacts are

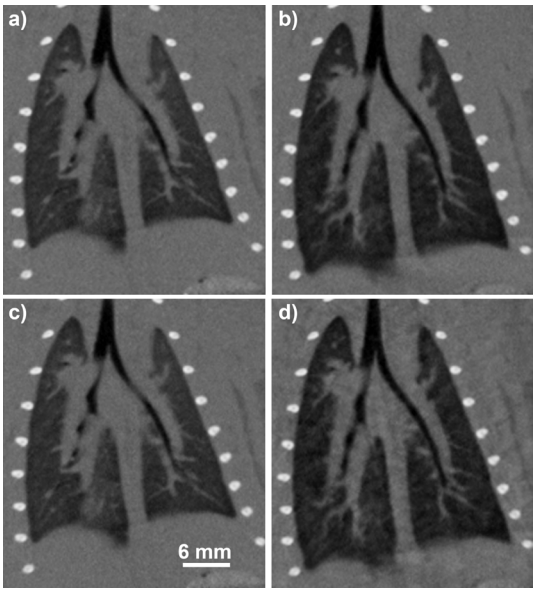

Figure 2. Coronal slices of a single rat reconstructed with a 0.15 mm voxel spacing using projections acquired during all ten gantry rotations at end expiration, panels (a) and (c), and at peak inspiration, panels (b) and (d). The bottom row, panels (c) and (d), use only the in-phase projections for reconstruction, whereas in the upper row, panels (a) and (b), the least error algorithm added nearly in-phase projections to fill all angular positions.

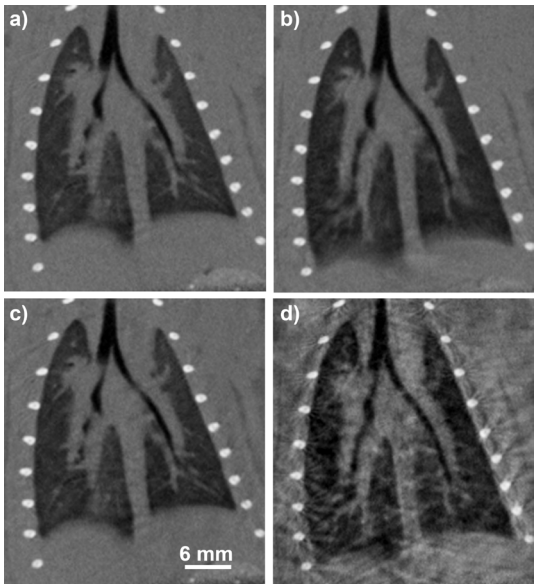

Figure 3. Coronal slices of a single rat reconstructed with a 0.15 mm voxel spacing using projections acquired during the first three gantry rotations at end expiration, panels (a) and (c), and at peak inspiration, panels (b) and (d). The bottom row, panels (c) and (d), use only the in-phase projections for reconstruction, whereas in the upper row, panels (a) and (b), the least error algorithm added nearly in-phase projections to fill all angular positions.

plotted in **Figure 5**. For the in-phase images, both the image noise and the missing view artefact measurements exhibited improved image quality for images reconstructed with more projections (including projections from more gantry rotations), as expected. The end expiration images were better than the corresponding peak inspiration images due to a larger number of available in-phase projections during end expiration. The rat respiratory traces showed that the period of end expiration is typically longer than peak inspiration, providing a longer temporal window for in-phase projections to be acquired. All in-phase images were compared with the 10-gantry rotation images using repeated measures ANOVA. No significant differences from the values measured in the 10-gantry rotation images were seen for images representing 6 or more gantry rotations for image noise and 7 or more gantry rotations for missing view artefacts. To ensure that the image quality is not reduced in the images, the scanning protocol could be altered to acquire projections over 7-gantry rotations instead of 10.

The least error reconstruction technique added nearly in-phase projections representing the view angles where no in-phase projection view was acquired. By completely filling projection space, the image noise was greatly reduced, and constant for all of the images regardless of respiratory phase or the number of gantry rotations included in the reconstructions. The missing view artefacts were completely eliminated. Comparing the least error images to the 10-rotation least error image showed no significant differences for image noise for 5 or more gantry rotations, and no differences in missing view artefacts.

Comparing the images within each dataset gives information about the variability of the measured values. To investigate the accuracy of the measured values, we considered the in-phase image reconstructed using projections from all 10-gantry rotations as the gold standard. Comparisons were made between the gold standard image and all of the images reconstructed using the least error method. Significant differences in the image noise and missing view artefacts were measured for all of the peak inspiration images, which is likely due to the large difference in the number of projections used to reconstruct the images. Since the end expiration images were already filling a large proportion of the projection angles, the missing view artefacts were not significantly different from the gold standard image reconstructed at end expiration. The image noise was significantly different for the 3-, 4-, and 5-rotation images only.

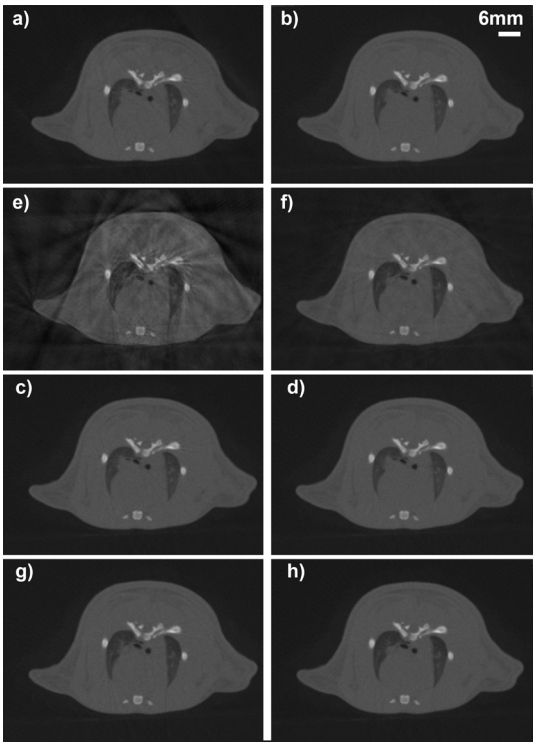

Figure 4. Axial images of a single rat reconstructed with 0.15 mm isotropic voxel spacing. End expiration images are in the top row: a) in phase, 3 rotations; b) in phase, 10 rotations; c) least error method, 3 rotations; and d) least error method, 10 rotations. Peak inspiration images are in the bottom row: e) in phase, 3 rotations; f) in phase, 10 rotations; g) least error method, 3 rotations; and h) least error method, 10 rotations. Notice the streaking around the outer surfaces of the rat and the bones, which disappear when all projection angles are filled (least error method).

3.4. Physiologically Relevant Measurements

The volumes of the lung, along with the mean CT number, are reported in **Table 1** (mean values and standard error in the mean). In some of the images, the seeded region-growing algorithm leaked, causing the extracted volume to include non-lung regions for the images made using only in-phase projections. This overestimation of the lung volume was more prevalent in the images made with fewer gantry rotations and affected primarily the peak inspiration images.

Comparing each in-phase image to the 10-rotation in-phase image, the physiologically relevant measured values yielded no statistically significant differences for 7 or more gantry rotations for end expiration for the metrics in **Table 1**. The peak inspiration images had no differences in lung volume or mean CT number. For the images using the least error method to fill all angles, there were no significant differences for 7 or more gantry rotations at peak inspiration when compared with the 10-rotation least error image for all physiologically-relevant measurements. The end expiration images showed no change in volume or CT number with increasing the number of gantry rotations.

To assess the accuracy, the least error images were compared to the gold standard image (10-rotation in-phase image). For peak inspiration, there were significant differences in the measured values for lung volume in the 3- to 6-rotation images. The measured values were smaller for the peak inspiration least error images (ranging from 5.74 mL to 6.08 mL vs. 6.30 mL for the in-phase 10 rotation gold standard), which is likely due to including nearly in-phase projections that have less air in the lungs representing inhalation or exhalation. The CT number

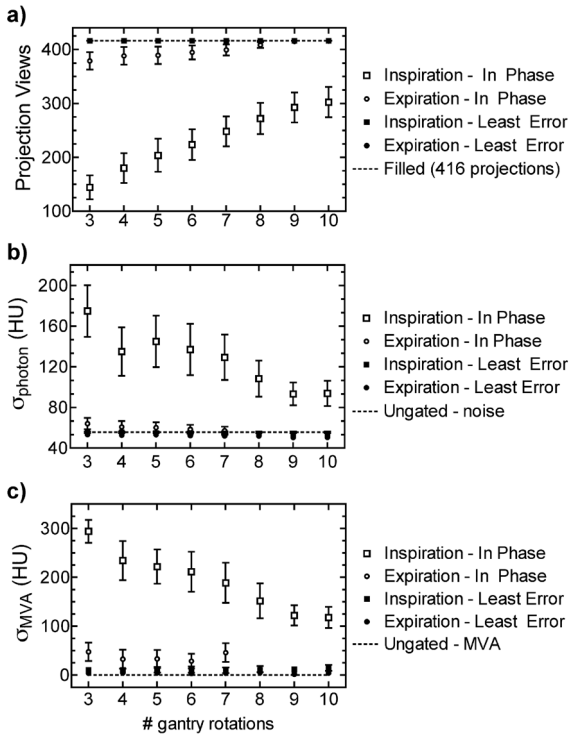

Figure 5. Image quality measurements plotted as a function of the number of gantry rotations used to reconstruct the image, a) number of projection views; b) photon noise; and c) missing view artefacts. Symbols show the mean value for all 5 rats, error bars are the standard error in the mean, and the dashed line represents the value for an image with all projection angles filled or an ungated image.

measured in the lung at peak inspiration was significantly increased for all images when compared with the 10-rotation in-phase image (−526 HU to −561 HU compared with −615 HU for the in-phase gold standard image). No significant differences were found during end expiration.

3.5. Functional Measurements

Calculated values for tidal volume and functional residual capacity are tabulated in **Table 2**. For comparisons within each dataset of the FRC, there was a significant difference for the in-phase reconstruction at 3 rotations and no significant differences in the least error reconstructions. Tidal volume showed no significant differences for the images reconstructed with only the in-phase projections, but a significant difference for 3- to 5-gantry rotations in the least error images.

Although the values for FRC and V_t were stable, there were significant differences for the tidal volume measurements for all rotations when the least error reconstructions were compared with the gold standard image (10 rotation, in-phase projections). The value measured in the 10-rotation images using only the in-phase projections is 1.71 mL, whereas the values in the images using the least error method ranged from 0.75 mL to 1.22 mL. The FRC demonstrated no significant differences from the gold standard image.

3.6. Assessing Diaphragm Motion

Plots were produced depicting all of the line profiles for 3- to 10-gantry rotations superimposed for each respiratory phase. **Figure 6** shows a single line profile from a coronal slice from the middle of the lungs for the 3-rotation, 10-rotation and ungated images. The line profile was obtained near the outer edge of the right lobe during 5a) end expiration and 5b) peak inspiration. The left graphs show the results from the reconstructions us-

Table 1. Physiological measurements from 5 rats (mean ± standard error in the mean). The asterisk* designates the measurements that are statistically different ($p < 0.05$) from the 10-rotation image within the dataset, and the dagger† designates a difference between the least error reconstruction and the 10-rotation in-phase image.

#Rot.	In-Phase Reconstruction End Expiration		Least Error Reconstruction End Expiration	
	Lung Volume [mL]	Lung CT Density [HU]	Lung Volume [mL]	Lung CT Density [HU]
3	4.67 ± 0.14*	−494 ± 11	4.67 ± 0.15	−486 ± 14
4	4.63 ± 0.15*	−488 ± 13	4.66 ± 0.13	−487 ± 12
5	4.61 ± 0.14	−489 ± 13	4.65 ± 0.14	−488 ± 15
6	4.63 ± 0.15*	−489 ± 13	4.61 ± 0.15	−484 ± 14
7	4.61 ± 0.14	−487 ± 13	4.61 ± 0.14	−485± 14
8	4.57 ± 0.15	−482 ± 11	4.71 ± 0.16	−484 ± 14
9	4.55 ± 0.14	−482 ± 12	4.56 ± 0.15	−481 ± 12
10	4.56 ± 0.14	−483 ± 13	4.55 ± 0.15	−480 ± 13
#Rot.	In-Phase Reconstruction Inspiration		Least Error Reconstruction Inspiration	
	Lung Volume [mL]	Lung CT Density [HU]	Lung Volume [mL]	Lung CT Density [HU]
3	5.95 ± 0.13	−596 ± 28	5.74 ± 0.08*†	−526 ± 7*†
4	6.15 ± 0.15	−620 ± 46	5.83 ± 0.07†	−533 ± 5*†
5	6.25 ± 0.15	−618 ± 37	5.88 ± 0.08†	−538 ± 5*†
6	6.33 ± 0.23	−634 ± 38	5.94 ± 0.07†	−542 ± 6*†
7	6.40 ± 0.25	−650 ± 47	6.00 ± 0.08	−547 ± 7†
8	6.24 ± 0.22	−614 ± 32	6.08 ± 0.12	−551 ± 8†
9	6.31 ± 0.22	−607 ± 29	6.08 ± 0.12	−555 ± 10†
10	6.30 ± 0.23	−615 ± 31	6.08 ± 0.13	−561 ± 10†

Table 2. Tidal volume and functional residual capacity measured in 5 rats (mean ± standard error in the mean). The asterisk* designates the measurements that are statistically different ($p < 0.05$) from the 10-rotation image within the dataset, and the dagger† designates a difference between the least error reconstruction and the 10-rotation in-phase image.

#Rot.	In-Phase Reconstruction		Least Error Reconstruction	
	Functional Residual Capacity [mL]	Tidal Volume [mL]	Functional Residual Capacity [mL]	Tidal Volume [mL]
3	2.31 ± 0.10*	1.26 ± 0.27	2.27 ± 0.12	0.75 ± 0.10*†
4	2.26 ± 0.11	1.60 ± 0.42	2.27 ± 0.10	0.84 ± 0.09*†
5	2.26 ± 0.11	1.64 ± 0.37	2.28 ± 0.12	0.89 ± 0.12*†
6	2.27 ± 0.11	1.79 ± 0.35	2.24 ± 0.12	0.98 ± 0.12†
7	2.25 ± 0.11	1.98 ± 0.44	2.24 ± 0.12	1.04 ± 0.12†
8	2.21 ± 0.10	1.67 ± 0.33	2.28 ± 0.10	1.07 ± 0.15†
9	2.19 ± 0.10	1.66 ± 0.31	2.20 ± 0.11	1.18 ± 0.14†
10	2.20 ± 0.10	1.71 ± 0.32	2.19 ± 0.11	1.22 ± 0.15†

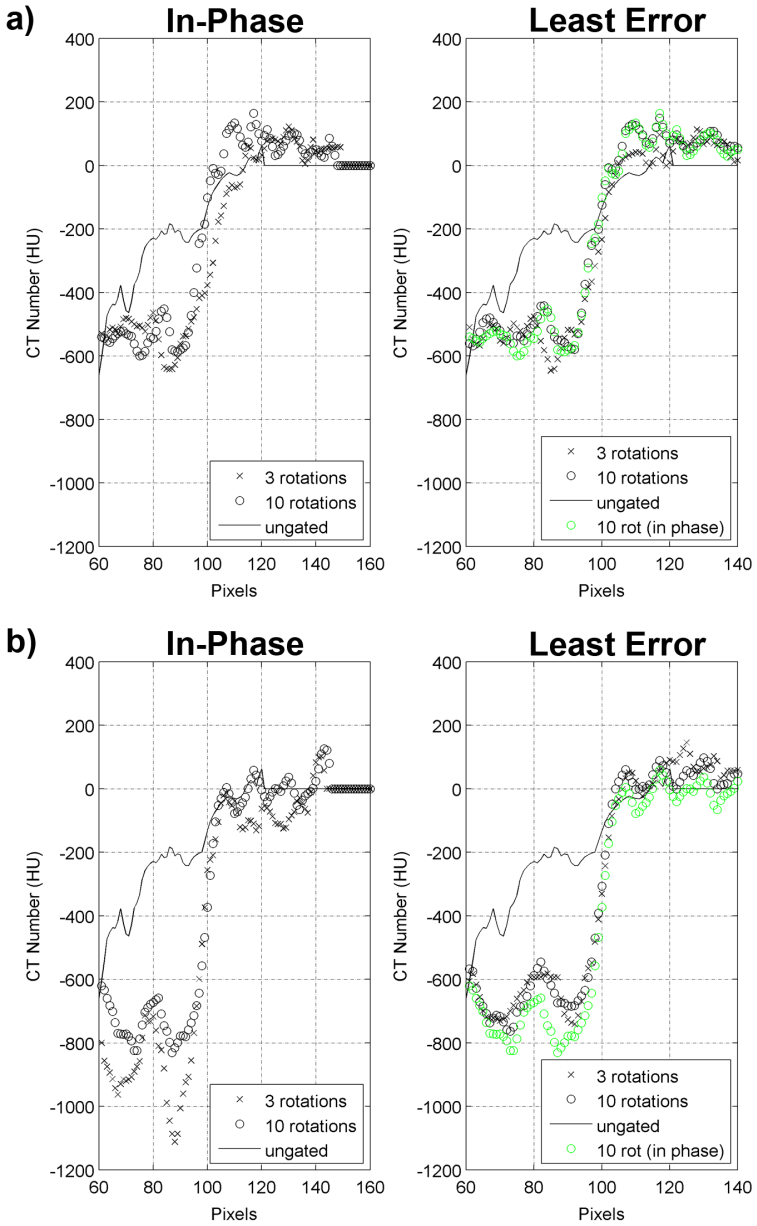

Figure 6. Line profile across the diaphragm near the outer edge of the right lobe in a coronal slice for a) end expiration and b) peak inspiration for a single rat. The left graph shows the profile from the image reconstructed using only in-phase projections, and the right graph includes additional projections that are nearly in-phase to fill all angular positions. The 10-rotation, in-phase curve is repeated on the right in green for comparison.

ing only the in-phase projections, and those on the right depict the images reconstructed with the least error approach, along with the 10-rotation in-phase curve in green for comparison. At both respiratory phases, the 10-rotation images exhibit sharper shoulders than the 3-rotation images. Comparing with the 10-rotation in-phase curve (in green), the deviations that are noticeable at the shoulders of the curves for the 3-rotation in-phase images are reduced in the least error images for both respiratory phases. In addition, the difference in the CT numbers is reduced for the least error images, indicating a slight reduction in the contrast between the lung and soft tissue at the edges of the diaphragm. These results suggest that adding in the nearly in-phase projections did cause blurring of the diaphragm, which was more obvious in the peak inspiration images and the images that had

a lower percentage of the angular positions filled with the in-phase projections. Although the diaphragm was not completely stationary in the images, adding the nearly in-phase views was still an improvement over the ungated images, and improved the images made with fewer gantry rotations.

The calculated slopes were compared to the 10-rotation, in-phase gold standard image for each respiratory phase separately. The steeper slope exhibited by the gated curves indicate the amount of improvement in diaphragm sharpness over the ungated images ($p < 0.01$ for both peak inspiration and end expiration). Only one rat exhibited significant differences during end expiration for the 3 - 5 rotations least error images for the maximum slope. For the other animals, the only significant differences were seen in the ungated image. No differences in the maximum slope were observed when the animals were grouped together, indicating that the maximum slope of the line profile across the diaphragm wasn't impacted by the number of gantry rotations used to formed the image or the projection sorting algorithm.

4. Discussion

In this study, we compared two retrospective respiratory-gating reconstruction approaches, using only the in-phase projections to form the image and a least error method to fill all angular positions. Completely filling all angular positions improved the image quality qualitatively, as demonstrated in **Figures 2** and **3**, and quantitatively as the measured photon noise and missing view artefacts were reduced, shown in **Figure 5**. This improvement in image quality permitted the use of an automated segmentation algorithm, namely seeded region growing, for extracting the lungs. This type of grey-scale based algorithm requires accurate CT numbers, low pixel-to-pixel variation and an artefact-free image. For the peak inspiration in-phase images, which had fewer in-phase views available for reconstruction, the algorithm could leak into the surrounding tissue, instead of selecting only the lung. By adding in the nearly in-phase views, the algorithm could correctly identify the margins of the target organ.

Measured values for the lung volume and the mean CT density in the lungs were compared for all of the images. The measured values for the inphase 10-rotation images were used as the gold standard; the observed values for tidal volume and respiratory rates are within the published range for healthy free-breathing adult rats of 1.5 mL and 85 breaths per minute respectively [29]. For both reconstruction techniques, the physiologically relevant measurements were not statistically different from the corresponding 10-rotation image for images using projection views from 7- or more gantry rotations. From the results in **Table 1**, it is clear that the measured lung volumes were systematically smaller for peak inspiration using the least error reconstruction compared to the images reconstructed with only the in-phase views. In addition, the measured values for CT density are significantly higher in the peak inspiration images for the least error images where all angular positions are filled. These systematic errors result from adding in the nearly in-phase views. The nearly in-phase images for the peak inspiration phase would be acquired at the end of inhalation or the beginning of exhalation. These views would have a reduced lung volume and air content compared to the projections acquired during peak inspiration. The result is a reduction in the lung volume and the air content in the lungs will be reduced, leading to a higher CT number (more positive). This underestimation of the air content in the lungs at peak inspiration is likely the main cause of the systematic reduction in calculated tidal volumes for the images reconstructed with all of projection space filled exhibited in **Table 2**.

For the purpose of reducing organ motion in the images, and for estimating anatomy from the images, the least error method should provide reliable measurements. The diaphragm analysis, displayed in **Figure 6**, shows that the diaphragm sharpness for the gated images is improved over the ungated images, but as more of the available projections are from the inhalation and exhalation portions of the respiratory cycle, which correspond to the times when the diaphragm is moving the most, the diaphragm sharpness is degraded at the shoulders of the graphs. The measured values for anatomical features, such as lung volume, are stable with no significant differences for reconstructions using 7 or more gantry rotations, although systematic errors are inevitable. To minimise the effects of these systematic errors, control animals should be included in each study so the relative measured values can be reported with the idea that the trends in the data will not be adversely affected by these systematic errors.

For studies that require functional information from the images, the systematic errors that occur for the peak inspiration images using the least error method combine to produce errors in the calculated tidal volume. The values tabulated for tidal volume, shown in **Table 2**, exhibit stable values within the dataset, with no significant differences noted for images reconstructed with data from more than 5 gantry rotations. However, the values for

the images reconstructed using the least error method produced a smaller value for the tidal volume than the images that used only the in-phase projections. The difference between the volumes and air content at peak inspiration and end expiration was smaller for the least error method due to the inclusion of nearly in-phase views. For the functional residual capacity, the effect is less pronounced because the images reconstructed during end expiration had a higher fraction that were in-phase compared to the peak inspiration case, leading to no significant differences in the calculated values between the two reconstruction approaches.

One factor that affected the peak inspiration images quite strongly was the limited number of angular positions for which in-phase projections were available. In our population of rats, there were a few scans where adding another gantry rotation only increased the number of in-phase projections by a small number, which was particularly problematic for the peak inspiration phase, as it is much shorter than end expiration. In these cases, we believe that the respiration period of the rat synchronized with the gantry rotation time, causing subsequent projections to be acquired during the identical respiratory phase. Therefore, increasing the scan time, and associated dose, resulted in mainly redundant projections. Furthermore, the angular distribution of the projections did not even out as more data was included; in fact, one scan had insufficient angular coverage to produce a reliable image and was excluded from the study. The number of projections included for the in-phase reconstructions are shown in **Figure 5(a)**. Previous work in mice showed a steeper slope in the peak inspiration curve [12], which we believe is due to faster respiration in mice. Faster respiration will allow for more breaths to occur during the first gantry rotation, and provide an improved angular distribution of the in-phase projections. Furthermore, a fast respiration rate may ensure that the respiratory period would not remain synchronized with the rotation period for a significant portion of the rotation time. Other models of micro-CT scanners may not suffer from the exact same issues outlined here, as the rotation speed and optimized imaging parameters will vary by model. However, the concept of optimizing the protocols by balancing angular oversampling to achieve complete filling of projection space, and exquisite image quality, with the requirements to minimize the scan time, anaesthesia time and x-ray dose to the animal is applicable to all retrospectively respiratory-gated studies.

Optimization of the acquisition and reconstruction protocols is dependent upon the measurements that are required from the data. If functional information about the lung is required, the projections from 7 gantry-rotations should be reconstructed using only the in-phase projections. For this approach the exposure time would be reduced to 35 s with an entrance dose of 0.2 Gy. A coronal slice through one rat is included in **Figure 7** for the optimal 7-gantry rotation reconstruction using only the in-phase projection views acquired during a) end expiration, and b) peak inspiration. Alternatively, the least error reconstruction could be used with 7-rotations, with the knowledge that the tidal volume values will be slightly underestimated. Coronal slices through the same rat using the least error approach is shown in **Figure 7(c)** at end expiration and d) at peak inspiration.

The least error approach did offer an obvious benefit for image quality, and improved the outcomes of semi-automated image processing algorithms, such as seeded region growing for feature extraction. The main failure of this technique was for the peak inspiration images in measuring the lung CT number, which was too high, and the lung volume, which was too low. These systematic errors caused inaccuracies in the calculated functional information for the lung (tidal volume). Using a combined analysis approach, the lung boundaries and volumetric measurements could be derived from the least-error projection selection approach, and the density measurements could be obtained using the reconstructed images using the in-phase projections. There may be other applications where this systematic error would not be seen. For example, any object that is changing in volume throughout the cycle, but maintains a constant CT number may not suffer from the same errors. In particular, cardiac-gated imaging using a contrast agent may be well-suited for the least error reconstruction, as the chamber size would change in time, but the CT number of the blood would remain constant. Retrospectively cardiac-gated micro-CT is a task that suffers from severe artefacts, particularly when imaging the mouse heart due to the extremely short cardiac cycle (~25 - 30 ms). More *in vivo* testing is required to assess what tasks are well suited for the least error reconstruction.

Since the optimal number of gantry rotations is 7 for both reconstruction approaches, the image quality can be improved with no loss of important information at a modest x-ray dose to the animal. To assess functional parameters in free-breathing rats, both reconstruction techniques can be utilized with the 7-rotation dataset. Least error images can be used for display purposes and qualitative assessment for both respiratory phases, and can be quantitatively analysed for the lung volume, CT density and functional residual capacity using the end expiration images. For the corresponding peak inspiration measurements of lung volume, CT density and tidal volume, an image using only the in-phase projections should be reconstructed and analysed.

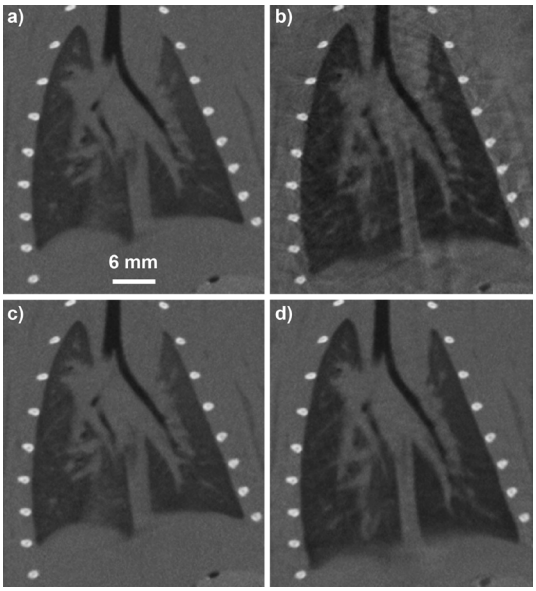

Figure 7. Coronal images from the same rat using the optimized protocol for both the in-phase and least error reconstruction techniques (7 gantry-rotations, 35 s exposure time, 0.2 Gy entrance dose). Projections from the first 7-gantry rotations were used to reconstruct only the in-phase views acquired during (a) end expiration and (b) peak inspiration. The same coronal slice from the 7-gantry-rotation image using the least error reconstruction shown during (c) end expiration and (d) peak inspiration. The reconstructed isotropic voxel spacing is 0.15 mm.

5. Conclusions

In this study, we compared a least error method of reconstructing retrospectively respiratory-gated micro-CT images that uses nearly in-phase projections to completely fill projection space with our previously published method using only in-phase projections. We evaluated the images based on image quality metrics, such as noise and missing view artefacts, and physiologically-relevant measurements, such as lung volume, CT density, tidal volume and functional residual capacity. Our comparisons show that improved image quality occurs when using the least error method to completely fill projection space, but some physiologically relevant measurements are systematically altered in the peak inspiration phase, leading to inaccuracies in the calculated tidal volume. The least error method may be better suited to measurements of organs that do not change their attenuation properties during the scan.

For motion reduction and anatomical measurements, using the least error method will provide reproducible measured values; however, control animals must be included and relative values are reported to eliminate systematic inaccuracies. For the free-breathing rats in our study, the desired measurements of physiology and function can be obtained with an imaging protocol of 7 gantry-rotations, which requires a 35 s exposure time and an entrance dose of 0.2 Gy for either the in-phase reconstruction or the least error reconstruction. By combining both of these techniques together, the image quality can be improved with no loss of accuracy in the physiologically relevant measurements by using both the least error and in-phase reconstructions to assess the peak inspiration images, whereas for the end expiration phase, the least error image is sufficient.

Acknowledgements

The authors wish to acknowledge Ivailo Petrov and Andrew Wheatley for the retrospective respiratory sorting code and Lynda McCaig for animal handling expertise. Dr. M. Drangova is a Career Investigator with the Heart and Stroke Foundation of Ontario. Financial support for this project was from the Ontario Thoracic Society, the

Ontario Ministry of Education and Training (Ontario Work Study Program), Ryerson University (University Work Study Program), NSERC Discovery Grant and University of British Columbia (Work Study Program).

References

[1] Lederlin, M., Ozier, A., Montaudon, M., *et al.* (2010) Airway Remodeling in a Mouse Asthma Model Assessed by *in Vivo* Respiratory-Gated Micro-Computed Tomography. *European Radiology*, **20**, 128-137. http://dx.doi.org/10.1007/s00330-009-1541-0

[2] Cody, D.D., Nelson, C.L., Bradley, W.M., *et al.* (2005) Murine Lung Tumor Measurement Using Respiratory-Gated Micro-Computed Tomography. *Investigative Radiology*, **40**, 263-269. http://dx.doi.org/10.1097/01.rli.0000160070.67270.05

[3] Ford, N.L., Martin, E.L., Lewis, J.F., *et al.* (2009) Quantifying Lung Morphology with Respiratory-Gated Micro-CT in a Murine Model of Emphysema. *Physics in Medicine and Biology*, **54**, 2121-2130. http://dx.doi.org/10.1088/0031-9155/54/7/018

[4] Froese, A.R., Ask, K., Labiris, R., *et al.* (2007) Three-Dimensional Computed Tomography Imaging in an Animal Model of Emphysema. *European Respiratory Journal*, **30**, 1082-1089. http://dx.doi.org/10.1183/09031936.00000507

[5] Zhou, Z., Kozlowski, J. and Schuster, D.P. (2005) Physiologic, Biochemical, and Imaging Characterization of Acute Lung Injury in Mice. *American Journal of Respiratory and Critical Care Medicine*, **172**, 344-351. http://dx.doi.org/10.1164/rccm.200503-343OC

[6] Johnson, K.A. (2007) Imaging Techniques for Small Animal Imaging Models of Pulmonary Disease: Micro-CT. *Toxicologic Pathology*, **35**, 59-64. http://dx.doi.org/10.1080/01926230601184262

[7] Thiesse, J., Namati, E., Sieren, J., *et al.* (2010) Lung Structure Phenotype Variation in Inbred Mouse Strains Revealed through *in Vivo* Micro-CT Imaging. *Journal of Applied Physiology*, **109**, 1960-1968. http://dx.doi.org/10.1152/japplphysiol.01322.2009

[8] Cavanaugh, D., Johnson, E., Price, R.E., *et al.* (2004) *In Vivo* Respiratory-Gated Micro-CT Imaging in Small-Animal Oncology Models. *Molecular Imaging*, **3**, 55-62. http://dx.doi.org/10.1162/153535004773861723

[9] Walters, E.B., Panda, K., Bankson, J.A., *et al.* (2004) Improved Method of *in Vivo* Respiratory-Gated Micro-CT Imaging. *Physics in Medicine and Biology*, **49**, 4163-4172. http://dx.doi.org/10.1088/0031-9155/49/17/023

[10] Ford, N.L., Nikolov, H.N., Norley, C.J., *et al.* (2005) Prospective Respiratory-Gated Micro-CT of Free Breathing Rodents. *Medical Physics*, **32**, 2888-2898. http://dx.doi.org/10.1118/1.2013007

[11] Namati, E., Chon, D., Thiesse, J., *et al.* (2006) *In Vivo* Micro-CT Lung Imaging via a Computer-Controlled Intermittent Iso-Pressure Breath Hold (IIBH) Technique. *Physics in Medicine and Biology*, **51**, 6061-6075. http://dx.doi.org/10.1088/0031-9155/51/23/008

[12] Ford, N.L., Wheatley, A.R., Holdsworth, D.W., *et al.* (2007) Optimization of a Retrospective Technique for Respiratory-Gated High Speed Micro-CT of Free-Breathing Rodents. *Physics in Medicine and Biology*, **52**, 5749-5769. http://dx.doi.org/10.1088/0031-9155/52/19/002

[13] Hu, J., Haworth, S.T., Molthen, R.C., *et al.* (2004) Dynamic Small Animal Lung Imaging via a Postacquisition Respiratory Gating Technique Using Micro-Cone Beam Computed Tomography. *Academic Radiology*, **11**, 961-970. http://dx.doi.org/10.1016/j.acra.2004.05.019

[14] Ertel, D., Kyriakou, Y., Lapp, R.M., *et al.* (2009) Respiratory Phase-Correlated Micro-CT Imaging of Free-Breathing Rodents. *Physics in Medicine and Biology*, **54**, 3837-3846. http://dx.doi.org/10.1088/0031-9155/54/12/015

[15] Artaechevarria, X., Perez-Martin, D., Ceresa, M., *et al.* (2009) Airway Segmentation and Analysis for the Study of Mouse Models of Lung Disease Using Micro-CT. *Physics in Medicine and Biology*, **54**, 7009-7024. http://dx.doi.org/10.1088/0031-9155/54/22/017

[16] De Backer, J.W., Vos, W.G., Burnell, P., *et al.* (2009) Study of the Variability in Upper and Lower Airway Morphology in Sprague-Dawley Rats Using Modern Micro-CT Scan-Based Segmentation Techniques. *Anatomical Record* (*Hoboken*), **292**, 720-727. http://dx.doi.org/10.1002/ar.20877

[17] Dame Carroll, J.R., Chandra, A., Jones, A.S., *et al.* (2006) Airway Dimensions Measured from Micro-Computed Tomography and High-Resolution Computed Tomography. *European Respiratory Journal*, **28**, 712-720. http://dx.doi.org/10.1183/09031936.06.00012405

[18] Ford, N.L., Martin, E.L., Lewis, J.F., *et al.* (2007) *In Vivo* Characterization of Lung Morphology and Function in Anaesthetized Free-Breathing Mice Using Non-Invasive Micro-Computed Tomography. *Journal of Applied Physiology*, **102**, 2046-2055. http://dx.doi.org/10.1152/japplphysiol.00629.2006

[19] Shingrani, R., Krenz, G. and Molthen, R. (2010) Automation Process for Morphometric Analysis of Volumetric CT Data from Pulmonary Vasculature in Rats. *Computer Methods and Programs in Biomedicine*, **97**, 62-77.

http://dx.doi.org/10.1016/j.cmpb.2009.07.009

[20] Armitage, S.E.J., Detombe, S.A., Pollmann, S.I., *et al.* (2012) Least-Error Projection Sorting to Optimize Retrospectively Gated Cardiac Micro-CT of Free-Breathing Mice. *Medical Physics*, **39**, 1452-1462. http://dx.doi.org/10.1118/1.3681949

[21] Du, L.Y., Lee, T.-Y. and Holdsworth, D.W. (2006) Image Quality Assessment of a Pre-Clinical Flat-Panel Volumetric Micro-CT Scanner. San Diego, 614216-8.

[22] Ross, W., Cody, D.D. and Hazle, J.D. (2006) Design and Performance Characteristics of a Digital Flat-Panel Computed Tomography System. *Medical Physics*, **33**, 1888-1901. http://dx.doi.org/10.1118/1.2198941

[23] Du, L.Y., Umoh, J., Nikolov, H.N., *et al.* (2007) A Quality Assurance Phantom for the Performance Evaluation of Volumetric Micro-CT Systems. *Physics in Medicine and Biology*, **52**, 7087-7108. http://dx.doi.org/10.1088/0031-9155/52/23/021

[24] Feldkamp, L.A., Davis, L.C. and Kress, J.W. (1984) Practical Cone-Beam Algorithm. *Journal of the Optical Society of America a-Optics Image Science and Vision*, **1**, 612-619.

[25] Otsu, N. (1979) A Threshold Selection Method from Gray-Level Histograms. *IEEE Transactions on Systems, Man, and Cybernetics*, **9**, 62-66. http://dx.doi.org/10.1109/TSMC.1979.4310076

[26] Mitzner, W., Brown, R. and Lee, W. (2001) *In Vivo* Measurement of Lung Volumes in Mice. *Physiology Genomics*, **4**, 215-221.

[27] Brower, R., Wise, R.A., Hassapoyannes, C., *et al.* (1985) Effect of Lung Inflation on Lung Blood Volume and Pulmonary Venous Flow. *Journal of Applied Physiology*, **58**, 954-963.

[28] Guerrero, T., Castillo, R., Sanders, K., *et al.* (2006) Novel Method to Calculate Pulmonary Compliance Images in Rodents from Computed Tomography Acquired at Constant Pressures. *Physics in Medicine and Biology*, **51**, 1101-1112. http://dx.doi.org/10.1088/0031-9155/51/5/003

[29] Suckow, M.A., Weisbroth, S.H. and Franklin, C.L. (2005) The Laboratory Rat. Elsevier Science.